Computational Physics Lab 1: Numerical investigation of waves in a one-dimensional shallow water model

Augustin Ionescu

November 7, 2017

1 Introduction

This report investigates the behaviour of waves in a one-dimensional shallow water model by using a Matlab script to numerically solve the equations involved. It starts with a linearised version of the shallow water differential equations and analyses the evolution of the system both mechanically and energetically under periodic and open boundary conditions. This is realized by implementing an Euler forward step and a "leapfrog" scheme in the Matlab code. The complete, non-linear system, is then considered and again analysed under the two sets of boundary conditions, including the more complex case of orography.

2 Background

2.1 Shallow water equations

The shallow water equations, which are derived from the Navier-Stokes equations under the assumption that the horizontal length scale is much larger than the vertical one, are a set of hyperbolic partial differential equations that describe the evolution of a hydrostatic homogeneous incompressible fluid in response to gravitational and rotational accelerations. [1] The one-dimensional equations are used extensively in computer models because they are significantly easier to solve than the full shallow water equations. For a model without Earths rotation (f = 0 i.e. no Coriolis force), they are expressed as:

$$\frac{\partial u}{\partial t} + u\frac{\partial u}{\partial x} + g\frac{\partial h}{\partial x} = 0 \tag{1}$$

$$\frac{\partial h}{\partial t} + u\frac{\partial h - h_B}{\partial x} + (h - h_B)\frac{\partial u}{\partial x} = 0 \tag{2}$$

where u is the velocity in x-direction, h is the height of the surface of the water layer and $h_B = h_B(x)$ describes the topography of the ground. [2]

2.2 Numerical integration

In general, differentials can be transformed to centred differences, forward differences and backward differences, respectively:

$$\frac{\partial X_m^n}{\partial t} \to \frac{X_m^{n+1} - X_m^{n-1}}{2\Delta t} \quad \text{and} \quad \frac{\partial X_m^n}{\partial x} \to \frac{X_{m+1}^n - X_{m-1}^n}{2\Delta x} \tag{3}$$

$$\frac{\partial X_m^n}{\partial t} \rightarrow \frac{X_m^{n+1} - X_m^n}{\Delta t} \quad \text{and} \quad \frac{\partial X_m^n}{\partial x} \rightarrow \frac{X_{m+1}^n - X_m^n}{\Delta x} \tag{4}$$

$$\frac{\partial X_m^n}{\partial t} \rightarrow \frac{X_m^n - X_m^{n-1}}{\Delta t} \quad \text{and} \quad \frac{\partial X_m^n}{\partial x} \rightarrow \frac{X_m^n - X_{m-1}^n}{\Delta x} \tag{5}$$

The Euler forward step uses a forward difference in time and a centred difference in space. The leapfrog forward step uses centred differences in both space and time. [3]

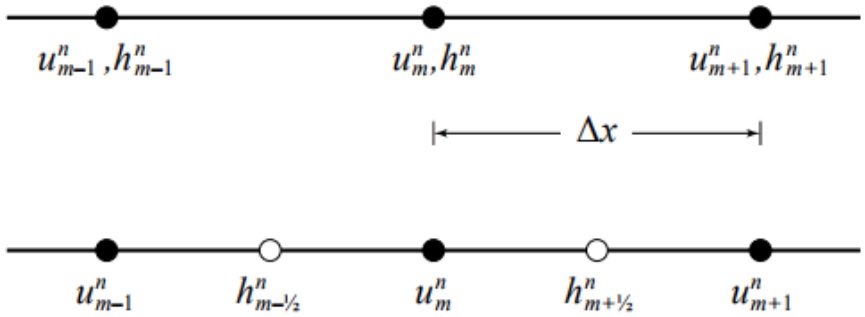

Figure 1: The normal (top) versus the staggered (bottom) grid.

In this project, in order to improve the numerical integration, calculations are performed on a staggered grid on which different variables (such as the disturbances in speed u' and height h') are defined at different grid points. Figure 1 shows a staggered grid on which grid points for h' are shifted by $\frac{1}{2}x$ to the left of u'.

Also, to assure that the numerical integration is stable, the Courant-Friedrichs-Lewy (CFL) condition needs to be fulfilled as

$$CFL = c\frac{t}{x} \tag{6}$$

with $c = \sqrt{gH}$. Knowing the CFL conditions hence allows to determine the maximum possible time step Δt for stable integration for a given distance Δx between grid points.

3 Methodology

3.1 Linearisation

The system in Equations 1 and 2 is first linearised by assuming that velocity and height can be split into a mean value and a fluctuation as $u = U + u'$ and $h = H + h'$, respectively, with $U, H = const$ and $h_B \ll H$:

$$\frac{\partial u'}{\partial t} + (U + u')\frac{\partial u'}{\partial x} + g\frac{\partial h'}{\partial x} = 0 \quad \text{and} \quad \frac{\partial h'}{\partial t} + (U + u')\frac{\partial h' - \partial h_B}{\partial x} + (H + h' - h_B)\frac{\partial u'}{\partial x} = 0 \tag{7}$$

By considering that vanishingly small products such as $u'\frac{\partial u'}{\partial x} \to 0$, the resulting linear system will look as follows

$$\boxed{\frac{\partial u'}{\partial t} + U\frac{\partial u'}{\partial x} + g\frac{\partial h'}{\partial x} = 0} \tag{8}$$

$$\boxed{\frac{\partial h'}{\partial t} + U\frac{\partial h' - \partial h_B}{\partial x} + (H - h_B)\frac{\partial u'}{\partial x} = 0} \tag{9}$$

3.2 Numerical differences

The linear system of Equations 8 and 9 can then be transformed from differential to differences so that it can be numerically solved. Assuming the simplest possible case without orographic forcing (i.e. $h_B = 0$) and applying Eqns. 3- 5 on a staggered grid, the system will look as below.

For Euler forward step (forward difference in time, centred difference in space):

$$\boxed{\frac{(u')_m^{n+1} - (u')_m^n}{\Delta t} + U\left(\frac{(u')_{m+1}^n - (u')_{m-1}^n}{2\Delta x}\right) + g\left(\frac{(h')_{m+1/2}^n - (h')_{m-1/2}^n}{2\Delta x}\right) = 0} \tag{10}$$

$$\boxed{\frac{(h')_{m+1/2}^{n+1} - (h')_{m+1/2}^n}{\Delta t} + U\left(\frac{(h')_{m+3/2}^n - (h')_{m-1/2}^n}{2\Delta x}\right) + H\left(\frac{(u')_{m+1}^n - (u')_m^n}{\Delta x}\right) = 0} \tag{11}$$

For "leapfrog" scheme (centred differences in both space and time):

$$\boxed{\frac{(u')_m^{n+1} - (u')_m^{n-1}}{2\Delta t} + U\left(\frac{(u')_{m+1}^n - (u')_{m-1}^n}{2\Delta x}\right) + g\left(\frac{(h')_{m+1/2}^n - (h')_{m-1/2}^n}{2\Delta x}\right) = 0} \tag{12}$$

$$\boxed{\frac{(h')_{m+1/2}^{n+1} - (h')_{m+1/2}^{n-1}}{2\Delta t} + U\left(\frac{(h')_{m+3/2}^n - (h')_{m-1/2}^n}{2\Delta x}\right) + H\left(\frac{(u')_{m+1}^n - (u')_m^n}{\Delta x}\right) = 0} \tag{13}$$

3.3 Numerical integration for periodic boundary conditions

Numerical integration is done on a staggered grid in a Matlab script, within a region $0 \leq x \leq L$ and by setting $h_B = 0$. The script uses a first Euler forward step followed by the application of the leapfrog scheme for the subsequent steps. The initial distortion is defined as

$$u'(x, t = 0) = 0 \tag{14}$$

$$h'(x, t = 0) = \begin{cases} 9^4 h_0 \left[\left(\frac{x}{L} - \frac{1}{2}\right)^2 - \left(\frac{1}{9}\right)^2\right]^2 & |\frac{x}{L} - \frac{1}{2}| \leq \frac{1}{9} \\ 0 & \text{otherwise} \end{cases} \tag{15}$$

with the length of the region $L = 100$ m, the height of the water layer $H = 10$ m, the ground stream velocity $U = 5$ m/s and the amplitude of the distortion $h_0 = 0.5$ m. The distance between grid points is set to $\Delta x = 0.25$ m and $CFL = 0.4$. The script is run for a total time of 15 s and a thorough investigation of how the waves are dispersing is presented in the Results section.

3.4 Numerical integration for open boundaries

Open boundary conditions are then introduced, meaning that the waves can leave the considered region at the left and right boundaries. [2] In the case of $U < c = \sqrt{gH}$, this is achieved for the left and right borders, respectively, as

$$x = 0 \begin{cases} \dfrac{\partial u'}{\partial t} + (U - c)\dfrac{\partial u'}{\partial x} = 0 \\ \dfrac{\partial h'}{\partial t} + (U - c)\dfrac{\partial h'}{\partial x} = 0 \end{cases} \tag{16}$$

and

$$x = L \begin{cases} \dfrac{\partial u'}{\partial t} + (U + c)\dfrac{\partial u'}{\partial x} = 0 \\ \dfrac{\partial h'}{\partial t} + (U + c)\dfrac{\partial h'}{\partial x} = 0 \end{cases} \tag{17}$$

Using an Euler forward step for the tendencies at the borders, the formulation in differences will be as follows

For $x = 0$:

$$\frac{(u')_m^{n+1} - (u')_m^n}{\Delta t} + (U - c)\left(\frac{(u')_{m+1}^n - (u')_m^n}{\Delta x}\right) = 0 \tag{18}$$

$$\frac{(h')_{m+1/2}^{n+1} - (h')_{m+1/2}^n}{\Delta t} + (U - c)\left(\frac{(h')_{m+3/2}^n - (h')_{m+1/2}^n}{\Delta x}\right) = 0 \tag{19}$$

For $x = L$:

$$\frac{(u')_m^{n+1} - (u')_m^n}{\Delta t} + (U + c)\left(\frac{(u')_m^n - (u')_{m-1}^n}{\Delta x}\right) = 0 \tag{20}$$

$$\frac{(h')_{m+1/2}^{n+1} - (h')_{m+1/2}^n}{\Delta t} + (U + c)\left(\frac{(h')_{m+1/2}^n - (h')_{m-1/2}^n}{\Delta x}\right) = 0 \tag{21}$$

These are then implemented in the script for the linearised model without orography and the details are presented in the Results section.

3.5 Energy

In the case of the linear system the energy is described as

$$E_{lin} = \frac{(u')^2}{2} + \frac{g}{H} \cdot \frac{(h')^2}{2} \tag{22}$$

while for the complete, non-linear system, the energy is described by

$$E_{nonlin} = (H + h')\frac{(u')^2}{2} + g\frac{(h')^2}{2} \tag{23}$$

These calculations of energy are implemented in the script and ran for 15s and 30s respectively, for both periodic and open boundary conditions. The results of the investigation are presented in the Results section.

3.6 Orography implementation

Finally, the behaviour of the full, non-linear system, with open borders is studied for the case of an orographic forcing described as $h_B = h'(x, t = 0)$ from Eq. 15, while the initial disturbances $h'(x, t = 0), u'(x, t = 0)$ are both set to zero.

4 Results

4.1 Linear system with periodic boundary conditions

For the periodic boundary conditions and parameters described in Section 3.3, the dispersion of the waves over a time interval of 15s is presented in Figure 2.

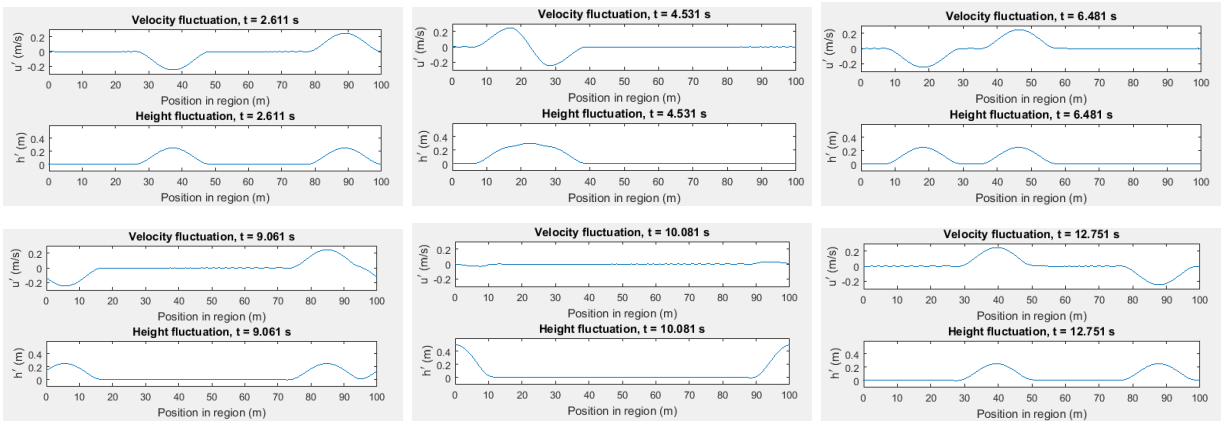

Figure 2: Evolution of the linear system under periodic boundary conditions

The longest possible time step for integration can be obtained from the CFL condition in Eq. 6 and was found to be $\Delta t_{max} = 0.0100964$. Running the script under changing parameters results in a different behaviour of the waves, which is presented in Table 1.

Table 1: Every table needs a caption.

Parameter change	Result
H increase	smaller velocity fluctuation, increased height fluctuation, waves meet at increased rate
U increase	waves meet at an increased rate, they catch up and overtake one another
h_0 increase	increased velocity and height fluctuation
g increase	increased velocity fluctuation

By only using the Euler forward step in the numerical integration, the calculation suddenly breaks. By decreasing the time step the result is a different scenario, in which the waves never meet and the velocity and height fluctuation have different, asymmetric, amplitudes as seen in Figure 3.

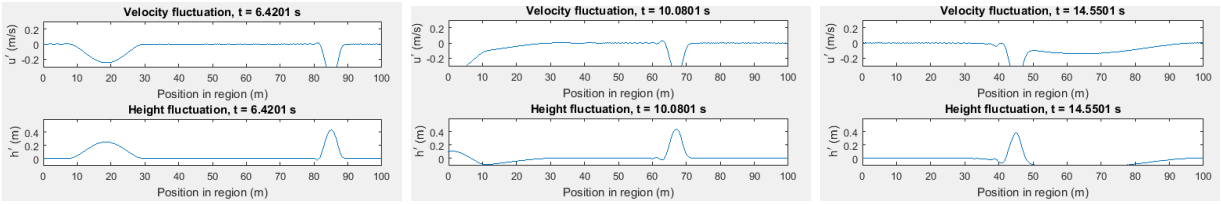

Figure 3: Evolution of the linear system under periodic boundary conditions by integration using Euler forward step

4.2 Linear system with open boundary conditions

In the case of open boundaries described in Section 3.4, the behaviour of the waves is presented in Figure 4, for a total time interval of 15s under the default parameters listed previously.

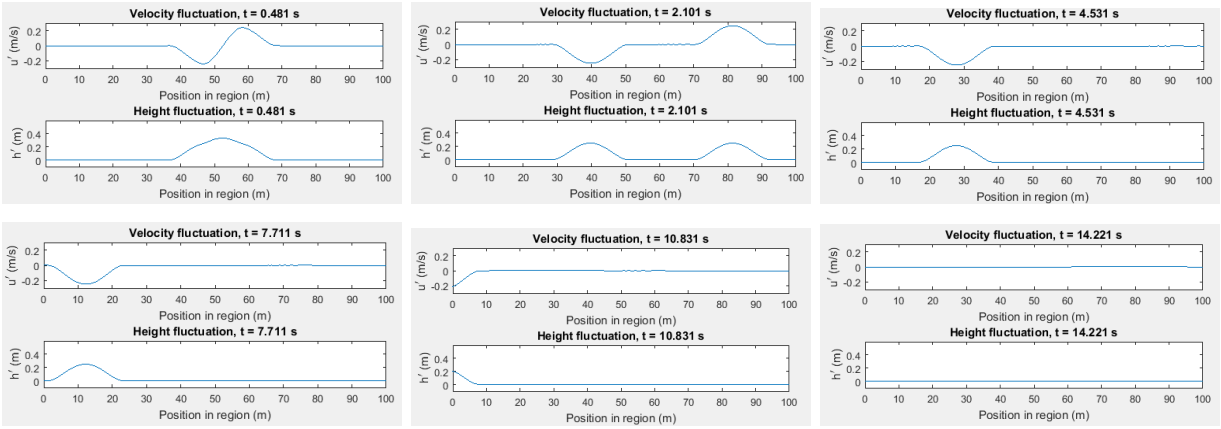

Figure 4: Evolution of the linear system under open boundary conditions

4.3 Energy of the linear system

Investigation of the change of energy in time for the linearised model with periodic and open boundaries was conducted and the results are presented in Figure 5.

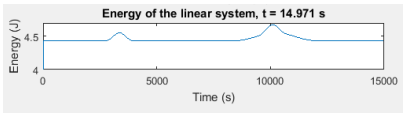

(a)

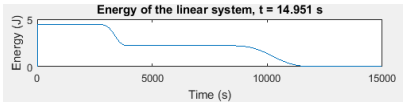

(b)

Figure 5: Change of energy over time for the linear system under (a) periodic and (b) open boundary conditions

It can be noted that while in the periodic boundary case the increase in energy is happening when the two waves meet, in the open boundary situation the total energy of the system decreases each time a wave leaves the boundary.

4.4 Non-linear system with periodic and open boundary conditions

For the non-linear system case without orographic forcing, the script was ran over a time period of 15s under the default parameters. The behaviour of the waves for periodic boundary conditions is shown is Figure 6.

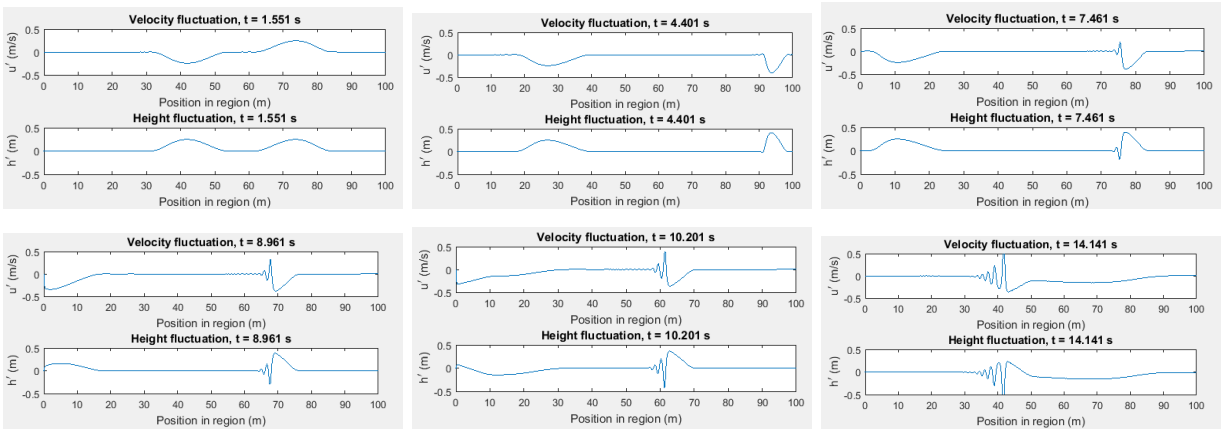

Figure 6: Evolution of the non-linear system under periodic boundary conditions

For the open boundary conditions, the wave dispersion is presented in Figure 7.

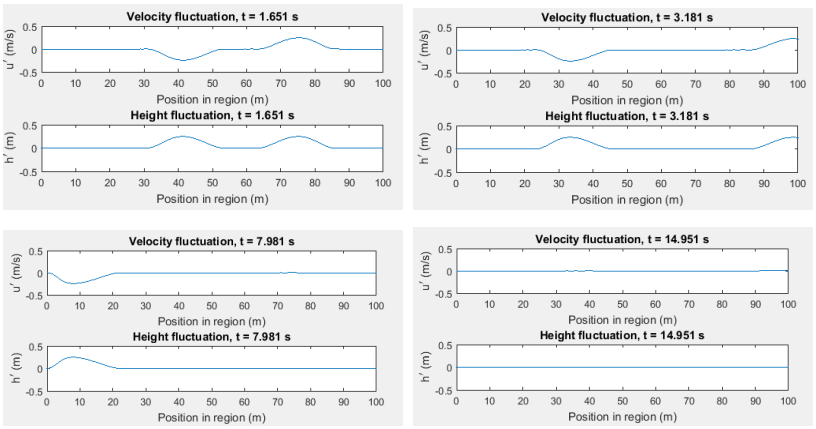

Figure 7: Evolution of the non-linear system under open boundary conditions without orography

In both situations the shape of the waves has a higher degree of asymmetry compared to the linear model, as expected from a more accurate scenario. After running the script for 30s under periodic boundary conditions, after adjusting the time step, the waves' behaviour appeared to maintain its periodic nature, which was not apparent previously, when it was ran for only 15s.

4.5 Non-linear system with orography

The full, non-linear system, was tested in the case of orographic forcing as described in Section 3.6 using open boundary conditions. The evolution of the system, including the energy change over time is presented in Figure 8.

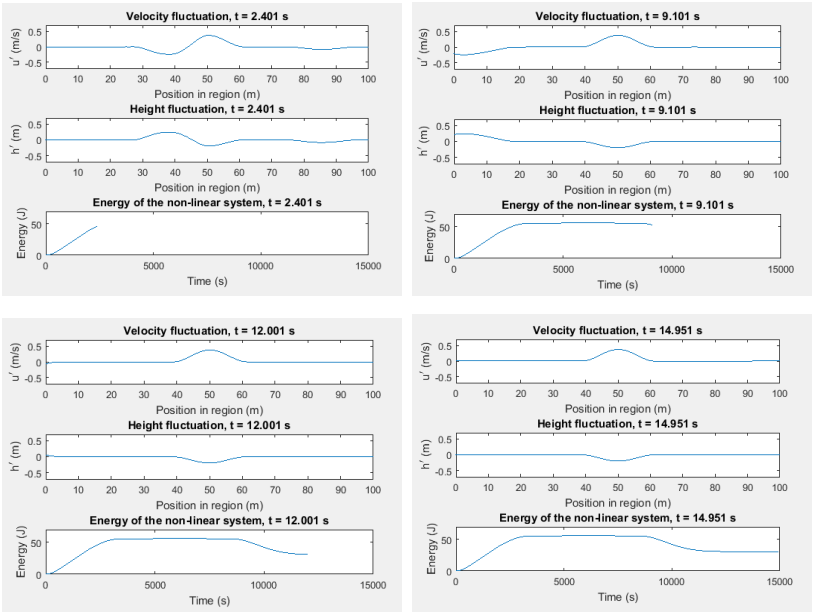

Figure 8: Evolution of the non-linear system under open boundary conditions with orography, including the energy evolution

5 Summary

In the case of periodic boundaries and no orographic forcing, it can be concluded that the energy of the system is kept constant except for the moments when the two waves meet. This is to be expected since with periodic boundaries, the waves do not leave the system in which we measure the energy. With open boundaries on the other hand, it can be concluded that energy is lost by the system as soon as a wave leaves the boundaries in between which the energy measurement is made, and the amount of energy lost depends on the height and speed of the wave. When orographic forcing is present, energy behaves in a similar manner, except for the fact that it is not entirely lost after the wave has left the boundary, which is to be expected due to the effect exerted by orography.

References

[1] Ming-Cheng Shiue, Jacques Laminie, Roger Temam, Joseph Tribbia, *Boundary value problems for the shallow water equations with topography*, Journal of Geophysical Research, Vol. 116, Issue C2, February 2011

[2] Holton, James R., *An introduction to dynamic meteorology*, Fourth Edition, International Geophysics Series, pp 535, Elsevier Academic Press, 2004.

[3] Trauth, Martin H., *MATLAB Recipes for Earth Sciences*, Springer, 2006.